Enzyme Electrokinetics: Hydrogen Evolution and Oxidation by *Allochromatium vinosum* [NiFe]-Hydrogenase†

Christophe Léger,‡,§ Anne K. Jones,‡ Winfried Roseboom,|| Simon P. J. Albracht,|| and Fraser A. Armstrong*,‡

Inorganic Chemistry Laboratory, Oxford University, South Parks Road, Oxford OX1 3QR, United Kingdom, and Swammerdam Institute for Life Sciences, Biochemistry, University of Amsterdam, Plantage Muidergracht 12, NL-1018 TV Amsterdam, The Netherlands

Received August 6, 2002; Revised Manuscript Received October 9, 2002

ABSTRACT: The mechanism of catalytic hydrogen evolution and oxidation by *Allochromatium vinosum* [NiFe]-hydrogenase has been studied by protein film voltammetry (PFV) with the enzyme adsorbed at a pyrolytic graphite edge electrode. By analyzing the entire shapes of catalytic voltammograms, the energetics of the catalytic cycles (reduction potentials and acidity constants of the active states), including the detailed profiles of activity against pH and the sequences of proton and electron transfers, have been determined, and these are discussed with respect to the mechanism. PFV, which probes rates as a continuous function of the electrochemical potential (i.e., in the "potential domain"), is proven to be an invaluable tool for determining the redox properties of an active site in the presence of its substrate, at room temperature, and during turnover. This is especially relevant in the case of the active states of hydrogenase, since one of its substrates (the proton) is always present at significant levels in the titration medium at physiological pH values.

Hydrogenases, which occur in both prokaryotic and lower eukaryotic species, catalyze the reversible two-electron interconversion of protons and hydrogen. Three different classes have been distinguished on the basis of metal content, i.e., [NiFe], Fe-only, and metal-free (*1*−*3*). Enzymes of the [NiFe] class consist of at least two subunits: a larger subunit (60 kDa) that contains the $NiFe(CN)_2(CO)$ active site and a smaller subunit (30 kDa) that houses at least one [4Fe4S] cluster. This conserved cluster is proximal, i.e., it lies in close proximity to the active site (within 12 Å). Additional FeS clusters are usually present in the small subunit to form an electron-transfer (ET)[1] pathway from the active site to the surface of the protein. In the prototypical [NiFe]-hydrogenases from *Desulfovibrio gigas* and *Allochromatium vinosum* (formerly *Chromatium vinosum*), this "wire" is completed by a "medial" [3Fe-4S] and a "distal" [4Fe-4S] cluster, the latter being the first cubane shown to be coordinated by a histidine ligand (*4*−*7*).

The active sites of the [NiFe]-hydrogenases from *D. gigas* and *A. vinosum* exist in a multitude of spectroscopically well-characterized redox states (Scheme 1) (*8*). Reduction produces an alternating series of EPR-active forms (marked with asterisks in Scheme 1) and EPR-silent forms. On the basis of Ni K-edge spectroscopy, they are thought to differ by no more than one electron at the Ni ion and thus to alternate between Ni^{III} and Ni^{II} states (*9*). Noting also that Mössbauer, electron paramagnetic resonance (EPR), and electron nuclear double resonance (ENDOR) spectroscopy suggest that the active-site Fe remains low-spin Fe^{II} throughout (*7*, *10*, *11*), the implication is that the active-site redox chemistry is not entirely based on the metal atoms in the [NiFe] fragment. While Ni_u*, Ni_u-S, Ni_r*, and Ni_r-S are inactive states that require reductive activation before catalytic activity can be observed, Ni_a-S, Ni_a-C*, and Ni_a-SR are catalytically active without any initial pretreatment. Despite all the structural, theoretical, and spectroscopic information available, the reaction mechanism remains a matter of debate and a very active area of investigation (see refs *3* and *12*−*15* for recent reviews).

Protein-film voltammetry (PFV), i.e., direct electrochemistry of protein molecules confined to an electrode surface, allows catalytic activity to be measured over a wide range

† This work was supported by funds from the UK EPSRC and BBSRC (Grants 43/B10492 and 43/E16711) and The Netherlands Organization for Scientific Research (NWO) Division for Chemical Science (CW). A.K.J. thanks the Rhodes Trust and the NSF for scholarships.

* To whom correspondence should be addressed: Phone 44-1865-272647; fax 44-1865-272690; e-mail fraser.armstrong@chem.ox.ac.uk.

‡ Oxford University.

§ Present address: Laboratoire de Bioénergétique et Ingénierie des Protéines, Marseille, France.

|| University of Amsterdam.

[1] Abbreviations: *A*, electrode area; CHES, 2-[*N*-cyclohexylamino]-ethenesulfonic acid; *E*, electrode potential; ET, electron transfer; $E_{X/Y}$, reduction potential of the redox couple X/Y, where $e_{X/Y} = \exp(f(E - E_{X/Y}))$ and $f = F/RT$; *F*, Faraday constant; Γ, electroactive coverage; HEPES, *N*-[2-hydroxyethyl]piperazine-*N*′-[2-ethanesulfonic acid]; *i*, current; i_{lim}, limiting current (at low potential); i_{-560} or i_{+240}, current recorded at −560 mV or +240 mV vs standard hydrogen electrode (SHE); k_0, first-order, interfacial electron transfer rate at zero overpotential; K_X, acidity constant of species X (to streamline the equations, the charge designation has been dropped from protons in the notations associated with the acidity constants); MES, 2-(*N*-morpholino)ethanesulfonic acid; *ν*, scan rate; ν_s, kinematic viscosity; *ω*, electrode rotation rate in units of revolutions per minute (rpm); PFV, protein film voltammetry; PGE, pyrolytic graphite edge; *R*, gas constant; *T*, temperature; TAPS, *N*-tris(hydroxymethyl)methyl-3-aminopropanesulfonic acid.

10.1021/bi026586e CCC: $22.00
Published on Web 12/05/2002

Scheme 1: Spectroscopically Characterized States of the Active Site of [NiFe]-Hydrogenases[a]

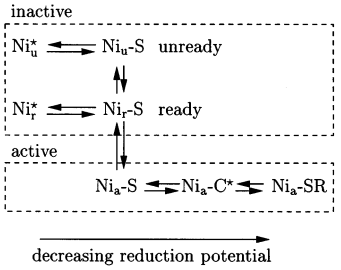

[a] Horizontal transitions denote redox processes with oxidation levels decreasing from left to right. The species in the upper box require activation before catalytic activity can be observed, whereas those in the lower box are active without pretreatment. Starred species show an $S = 1/2$ EPR signal from the NiFe active; the others are EPR-inactive. Subscripts u, r, and a refer to unready, ready, and active states, respectively. Different notations for the spectroscopically characterized states of [NiFe]-hydrogenases have been used over the years, and no consensus has emerged. We have chosen the nomenclature from ref *8*. An explanation of common, distinct notations and a summary of the spectroscopic (EPR and IR) characteristics of the different states can be found in ref *3*.

of electrochemical potential (*16*, *17*). Provided the enzyme can exchange electrons rapidly with the electrode, a catalytic current is observed that is directly proportional to the turnover rate and to the coverage of electroactive enzyme (Γ). Most significantly, and unique to this technique, the detailed potential dependence of the catalytic current reports directly on the energetics and kinetics of interconversions between different oxidation states of the enzyme during catalysis (*16*−*25*).

Previously, we have shown that *A. vinosum* [NiFe]-hydrogenase adsorbs at a pyrolytic graphite edge (PGE) electrode and that under a partial pressure of 0.1 bar of H_2 at 30 °C it catalyzes hydrogen oxidation with a turnover number exceeding 1500 s^{-1} (*25*). Indeed, the oxidative activity of the active site is comparable to that of a platinum fuel cell catalyst (*26*). The kinetics are clearly much faster than measured with soluble redox dyes as electron acceptors, indicating that in these more conventional solution experiments the rate is limited by the reaction with the dye (*25*). This has led us to conclude that PFV should be superior in terms of kinetic resolution, with the additional capability for precise potential control; thus, simply by using an instrument (an electrochemical workstation) to vary the electrode potential, the reaction $2H^+ + 2e^- \rightleftharpoons H_2$ can be driven in either direction, and rates can be measured and compared accurately. [Note that one of these redox substrates is inseparable from the solvent, making hydrogenase (water reduction) and photosystem II (water oxidation) special enzymes in this respect.] This is illustrated by the voltammogram shown in Figure 1, which has been recorded after immersion of a freshly polished, stationary (nonrotating) PGE electrode into a ca. 1 μM solution of *A. vinosum* [NiFe]-hydrogenase, and allowing the enzyme to adsorb to a saturating level. Two strong faradaic features, not observed in the absence of enzyme,[2] appear above the background

[2] The signals persist if the enzyme-coated electrode is transferred to a solution that does not contain enzyme, showing that the faradaic current results from the catalytic activity of the enzyme adsorbed on the electrode.

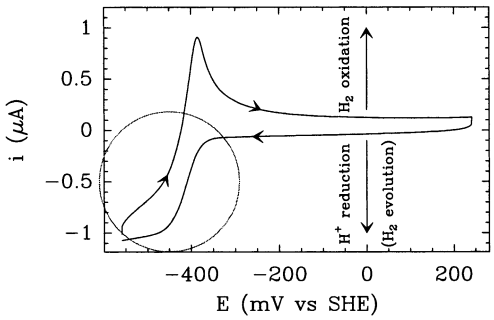

FIGURE 1: Cyclic voltammogram for an *A. vinosum* [NiFe]-hydrogenase film at a stationary PGE electrode under a nitrogen atmosphere. Arrows on the voltammetric trace show the direction of the sweep, and the circle indicates the part of the voltammogram corresponding to proton reduction. The solution, at 45 °C, pH 7, contains ca. 1 μM enzyme, 20 μg/mL polymyxin, 75 mM mixed buffer, and 0.1 M NaCl as supporting electrolyte. Scan rate: $\nu =$ 10 mV/s.

current: these are a reductive wave (negative current) and a corresponding peaklike oxidative signal (positive current) on the return scan (*25*). The reductive wave (circled) corresponds to reduction of the active site by the electrode and its continuous regeneration by proton reduction. The hydrogen that is produced accumulates near the electrode surface: its catalytic reoxidation results in the positive, peak-shaped signal observed as the electrode potential (E) is increased.

In this paper, we have used PFV to examine, quantitatively, the potential and pH dependence of the evolution *and* oxidation of hydrogen (i.e., catalysis in both directions) by *A. vinosum* [NiFe]-hydrogenase, and thereby gain a complementary perspective to that obtained from spectroscopic and more conventional kinetic studies. The potential-dependent activities, recorded directly as catalytic voltammograms, are interpreted to determine the reduction potentials of the active site under turnover conditions, the acidity constants of the different intermediates, and their contributions to the turnover rate in either direction. The results lead to catalytic cycles that describe interconversions between the different states of the active site, and also account for the inhibition of proton reduction by hydrogen and for the influence of pH on the catalytic activities for both proton reduction and hydrogen oxidation.

EXPERIMENTAL PROCEDURES

Samples of *A. vinosum* [NiFe]-hydrogenase were prepared as described in ref *27*.

Experiments were performed with solutions containing mixed buffers consisting of MES, HEPES, sodium acetate, TAPS, and CHES (15 mM or 2 mM of each component) and 0.1 M NaCl as supporting electrolyte. Mixtures were titrated with NaOH or HCl to the desired pH. Polymyxin B sulfate, a polyamine coadsorbate that stabilizes the protein film, was added from a stock solution of 20 mg/mL to give a final concentration of 200 μg/mL.

All experiments were carried out in a glovebox (Vacuum Atmospheres) under a N_2 atmosphere (O_2 < 4 ppm). The thermostated electrochemical cell (*28*) was housed in a Faraday cage. A PGE rotating-disk working electrode (area $A = 3$ mm^2) was used in conjunction with an EG&G M636 electrode rotator, a platinum wire was used as a counter-

electrode, and a saturated calomel electrode (SCE), located in a Luggin sidearm containing 0.1 M NaCl and maintained at room temperature, was used as a reference. All potentials are quoted versus the standard hydrogen electrode (SHE); $E_{SHE} = E_{SCE} + 241$ mV at 25 °C (*29*). Voltammetry was performed with an Autolab electrochemical analyzer (PGSTAT 20, Eco Chemie, Utrecht, The Netherlands) controlled by GPES software (Eco Chemie).

Before preparation of a film, the PGE electrode was polished with an aqueous alumina slurry (Buehler, 1 μm) and sonicated thoroughly. This generates a rough surface, rich in a variety of functionalities such as -COH and -COOH groups that interact with protein molecules (*16*). Protein films were prepared at 45 °C by adsorption from dilute solution (≈1 μM enzyme in pH 7 buffer): this was achieved by cycling the potential of the stationary electrode from −560 to +240 mV at a rate of 10 mV/s until a stable response (such as that shown in Figure 1) was obtained (*25*). After the enzyme solution was removed from the cell and replaced with enzyme-free buffer at pH 7, the electrode was held at −560 mV for 1 h at 45 °C to ensure that all the adsorbed enzymes molecules were activated (A. K. Jones, H. R. Pershad, S. P. J. Albracht, and F. A. Armstrong, manuscript in preparation). Care was then taken not to expose the film to oxidizing potentials that inactivate the enzyme.

Two types of electrochemical experiments were performed: these were cyclic voltammetry and measurements at a fixed potential. Cyclic voltammetry was used to determine the potential dependence of proton reduction and hydrogen oxidation activities. Fixed-potential measurements were carried out at −560 mV, and data at electrode rotation rates (ω) in the range 500−6000 rpm (ascending then descending) were collected, the aim being to determine the effect of substrate/product mass transport on the catalytic rates.

Experiments on either proton reduction or hydrogen oxidation were completed with the same film over the pH range 4−9 and at temperatures varying between 5 and 45 °C. With PFV, this simply involves transferring the electrode between different cell solutions, the pH values of which are subsequently remeasured at the experimental temperature. Approximately 60% of the electroactive coverage was lost during a set of experiments (about 15 different pH values over a period of several hours), and an identical series of experiments was completed for each pH, to allow for the resulting decrease in current with time. The following procedures were used:

Proton Reduction. Fixed-potential measurements were performed first in a standard buffer (pH ≈ 6.6), and then the current was remeasured at the pH of interest. Then cyclic voltammetry was performed at the same pH, and finally a fixed-potential measurement was made to monitor any changes in the electroactive coverage of the enzyme film.

Hydrogen Oxidation. Cyclic voltammograms at rotation rates 1000 and 2000 rpm were recorded sequentially for a standard buffer (pH ≈ 7.3), then for a solution at the pH of interest; the electrode was then returned to the standard buffer, to allow the change in activity to be normalized for changes in electroactive coverage.

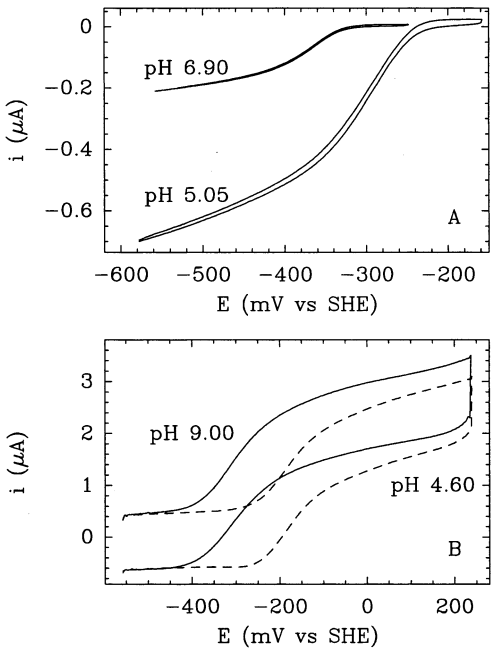

FIGURE 2: Catalytic voltammograms, for *A. vinosum* [NiFe]-hydrogenase adsorbed at a PGE rotating disk electrode. (A) Proton reduction under a N_2 atmosphere, electrode rotation rate $\omega = 6000$ rpm, in pH 5.05 (scan rate: $\nu = 6$ mV/s) and pH 6.90 ($\nu = 3$ mV/s) buffer. (B) Hydrogen oxidation at pH 9 (solid line) and 4.6 (dashed line), under 1 bar of H_2, $\omega = 2000$ rpm, $\nu = 200$ mV/s. In each case, the solution, at 5 °C, contains 20 μg/mL polymyxin, 75 mM mixed buffer, and 0.1 M NaCl.

RESULTS

Proton Reduction. Figure 2A shows rotating-disk voltammograms recorded under a N_2 atmosphere for a PGE electrode onto which *A. vinosum* [NiFe]-hydrogenase has been adsorbed. Comparison with Figure 1 shows that rotation of the electrode results in the disappearance of the oxidative peak, as the product of the reductive reaction (H_2) is swept away and dispersed. The resulting steady-state voltammogram is a plot of turnover number as a function of the driving force, and its shape and magnitude report on the relative activities and reduction potentials of the different redox states of the active site.

As a rule, the current should reach a limiting value at high driving force (i_{lim}), which corresponds to the activity of the fully reduced enzyme, and can be compared to results of solution assays with low-potential dyes. Figure 2 shows that this is not strictly the case, as there is a residual slope in the voltammograms at high driving force. This slope is small, as evident from Figure 2; therefore, for the following analysis of the dependence of the current on rotation rate, we made the approximation that the current recorded at −560 mV is close to the limiting value, i.e., $i_{-560} \approx i_{lim}$. While buffer concentration may affect proton availability, we noticed no differences in current magnitudes for experiments performed in 10 mM and 75 mM mixed buffer, and the analysis of the waveshape (vide infra) showed only small quantitative differences.

Figure 3A shows that the proton reduction current, recorded at −560 mV for two different pH values, increases with electrode rotation rate (ω). Normally in such cases, this results from the increased flux of substrate from the bulk solution to the electrode surface, and according to the Levich

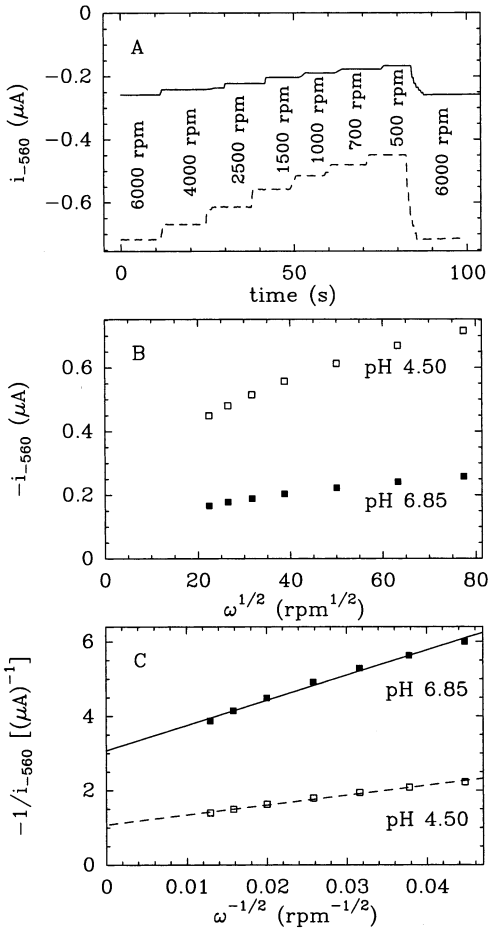

FIGURE 3: Dependence of proton reduction currents on electrode rotation rate. Current/rotation rate/time traces (A), Levich plots (B), and Koutecky−Levich plots (reciprocal current vs electrode rotation rate to the power −1/2) (C) at pH 4.50 (□ and dashed lines) and pH 6.85 (■ and solid lines) under a N_2 atmosphere are shown. Lines in panel C are fits to eq 1. The electrode was held at a potential of −563 mV vs SHE. Experimental conditions are as described in Figure 2.

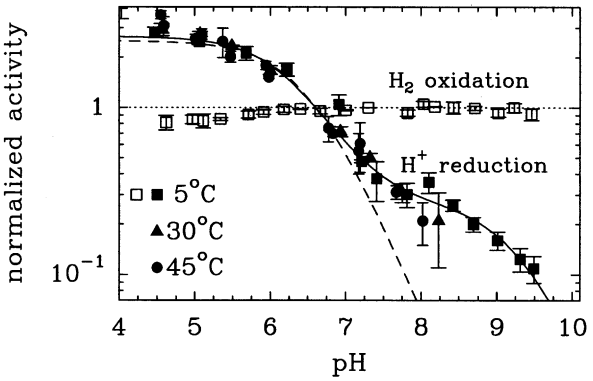

FIGURE 4: Relative pH dependences of the rates of hydrogen evolution (solid symbols) and oxidation (□). Solid symbols: relative reductive activity [$i_{-560}{}^{\omega=\infty}$(pH)/$i_{-560}{}^{\omega=\infty}$(pH = 6.6)] at infinite rotation rate as a function of pH at $E = -560$ mV. Dashed and solid lines are best fits to eqs 2 and 3, respectively. $T = 5$ °C (■), 30 °C (▲), and 45 °C (●); the other experimental conditions are as described in Figure 2. (□) Relative oxidative activity [i_{+240}(pH)/i_{+240}(pH = 7.3)] measured from the cyclic voltammograms recorded at 5 °C and $\omega = 2000$ rpm (reaction is not mass-transport-controlled). Error bars represent the difference between normalizing with respect to the current in a standard buffer before the experiment and normalizing with respect to the current in a standard buffer after the experiment.

equation, the current for a mass-transport-controlled reaction is proportional to $\omega^{1/2}$ (*29*). However, the Levich plots in Figure 3B show that the catalytic current levels off at high rotation rates, indicating that under these conditions, the activity is only slightly mass-transport-controlled. Good fits were obtained with the Koutecky−Levich equation (eq 1), which enables extrapolation to a finite current at infinite rotation rate (*25*, *28*, *30*):

$$\frac{1}{-i_{\mathrm{lim}}} = \frac{1}{-i_{\mathrm{lim}}{}^{\omega=\infty}} + \frac{1}{0.62nFAD^{2/3}\nu_{\mathrm{s}}{}^{-1/6}[\mathrm{H}^+]\omega^{1/2}} \quad (1)$$

In eq 1, $[H^+]$ represents the bulk concentration (actually activity) of protons, n is the number of electrons in the redox reaction (here, $n = 2$), F is the Faraday constant, A is the electrode area, D is the diffusion coefficient of the proton, and ν_s is the kinematic viscosity of the solution (*29*).

The small pH dependence of the slopes of the Koutecky−Levich plots in Figure 3C and the lack of dependence on buffer concentration contrasts with the strong $[H^+]^{-1}$ dependence predicted by eq 1. This argues against the idea that the rotation rate dependence of the limiting current is due to substrate (proton) depletion near the electrode surface. Nevertheless, the linear change as a function of $\omega^{-1/2}$ shows that a mass-transport process is influential, and this is most likely the dispersal of H_2 from the electrode surface to the bulk solution. Hydrogen is known to be an inhibitor of proton reduction (*25*, *31*), and this could be demonstrated easily by bubbling H_2 into the cell while maintaining the electrode potential at −560 mV vs SHE: this resulted (at pH 6, 5 °C) in a significant (at least 1 order of magnitude), instantaneous (seconds), and reversible loss of the proton reduction current.

Since the *y*-intercept of a Koutecky−Levich plot (Figure 3C) corresponds to the current extrapolated to infinite rotation rate ($i_{\mathrm{lim}}{}^{\omega=\infty}$), i.e., the maximum current attainable when mass transport is no longer limiting, the interpretation is that this relates to the catalytic rate of proton reduction in the absence of product inhibition. This quantity is proportional to the total amount of fully active enzyme present on the electrode ($A\Gamma$) and to the turnover number $i_{\mathrm{lim}}{}^{\omega=\infty}/2FA\Gamma$. It is difficult to quantify the electroactive coverage for *A. vinosum* [NiFe] films,[3] (*22*, *25*); however, assuming a maximum value for Γ of 3 pmol/cm^2, we determined *lower limits* of 50 and 500 s^{-1} for the turnover number corresponding to *uninhibited* proton reduction at 5 and 30 °C, respectively, at pH 4.5.

To correct the low-potential current ($i_{-560}{}^{\omega=\infty}$) for the decrease in electroactive coverage during the course of experiments, and to measure the intrinsic change in enzyme activity as a function of pH, each experiment carried out at a new pH was followed by remeasuring the activity in a

[3] The electroactive coverage (Γ) of a protein on an electrode is determined by integrating the current peak resulting from the stoichiometric redox transformation of a reliably assigned redox center (see, e.g., refs *22* and *25*). For an enzyme, this requires that the center is not catalytically cycling. Typically, noncatalytic signals are only faintly visible for *A. vinosum* [NiFe]-hydrogenase films, so that only an upper bound for Γ can be estimated (*25*) by use of the fact that one-electron, noncatalytic signals are expected to escape detection if the coverage is lower than about 3 pmol/cm^2.

standard pH buffer (6.6) thermostated at the same temperature. Normalization of $i_{-560}{}^{\omega=\infty}$ was performed relative to the current obtained in the standard buffer, both before and after the experiment (pH) of interest. The form of the resulting normalized activity profile, plotted in Figure 4 (filled symbols), shows little variation with temperature over the range 5−45 °C.

For cyclic voltammetry experiments (Figure 2A), a low scan rate was used to ensure that a catalytic steady state was maintained and to decrease the background (charging) current. In addition, the range of potential cycling was restricted so as to be more negative than the region in which the enzyme's active site is expected to convert to the inactive forms[4] (*32*), and the rotation rate was kept as high as practical considerations allowed (ω = 6000 rpm) to minimize the restriction due to mass transport (product dispersion) we have just mentioned. As Figure 2A shows, as the pH is decreased, the activity increases and the catalytic wave is significantly shifted to higher potentials.

Hydrogen Oxidation. Figure 2B shows cyclic voltamograms recorded under 1 bar of H_2 at 5 °C and two different pH values. A low temperature was used since the enzyme activity is very high and it was necessary to ensure that interfacial ET is not rate-limiting (*33*). To avoid the complication from oxidative inactivation,[4] a moderately fast scan rate (200 mV/s) was used so that the active site was kept at a high potential only for a few seconds during each scan, noting that oxidative inactivation is in any case slow at low temperatures (*27*). Rotating the electrode at 1000 or 2000 rpm did not change the electrochemical response; consequently it could be certain that the electrode rotation rate was fast enough to avoid hydrogen depletion near the electrode surface.

A large catalytic current is obtained at high potential, resulting from the continuous reoxidation of the H_2-reduced active site by interfacial ET. Comparison of panels A and B in Figure 2 shows that, at low pH and 5 °C, hydrogen oxidation at the high-potential limit is *about* 1 order of magnitude faster than proton reduction measured at the low-potential limit. (Note, however, that the electroactive coverage is unlikely to be the same for the particular experiments in panels A and B.) Figure 2B also shows that the position of the catalytic wave is pH dependent (as it is in the case of proton reduction). However, and by contrast with proton reduction, the *magnitude* of the limiting current, and thus the ability of the oxidized active site to catalyze hydrogen oxidation, seems not to depend on pH, once compensation has been made for the driving force. The variation in this *intrinsic* activity as a function of pH was quantified by measuring the current at the high-potential limit of each voltammogram (+240 mV vs SHE) and by normalizing this value with respect to the current measured immediately before or after the experiment in a standard buffer (pH 7.3). The corresponding activity profile is plotted (□) in Figure 4, from which it is clear that once the kinetics of electron uptake and the driving force are factored out, hydrogen oxidation activity is remarkably pH-independent.

Scheme 2: Generic Scheme for a Two-Electron Catalytic Reduction[a]

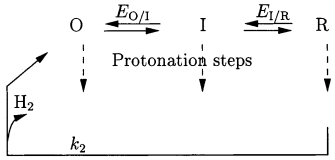

[a] The oxidized form of the active site is reduced to R (via an intermediate species I) following two one-electron transfers and coupled protonation steps. The reduced, substrate-bound form of the active site converts and releases the product with a rate k_2.

MODELING

Details of the modeling procedures used to analyze the catalytic waveshapes are given in the Supporting Information.

Proton Reduction: Catalytic Waveshape. Scheme 2 depicts the generic catalytic sequence that can account for the shape of the voltammograms. The oxidized form of the active site, termed O, is reduced in two successive, one-electron steps (via an intermediate oxidation level I) to R, which is protonated and releases H_2 with a rate k_2. (Later we will consider the correspondence with spectroscopically identified states.) The equation for the steady-state catalytic wave associated with this scheme was derived with the assumptions that protonation steps remain always at equilibrium and that the interfacial ET rates (these are assumed to be one-electron processes) can be described by the Butler−Volmer (BV) equation (*29*).

The first assumption is justified by the observation that the maximal H_2 oxidation rates greatly exceed those for proton reduction (Figure 2), which suggests that intramolecular proton transfer must be relatively fast. No assumptions were made regarding the order of protonation and reduction steps, which can be deduced a posteriori from the pH dependences of the best parameters of the fit.

The BV equation (*29*) is the simplest way to introduce the potential dependence of the rate of interfacial ET processes into the model. These phenomenological equations (eq S1 in the Supporting Information) predict the same potential dependence for interfacial ET rates as the Marcus theory, provided the driving force (the overpotential) is smaller than the reorganization energy of the redox process. (*16, 30, 34−36*). This is likely to be a good assumption in the present case, as the voltammograms were fit within a potential range of ±200 mV about the equilibrium potentials: this corresponds to a maximum driving force of 0.2 eV, whereas reported values for reorganization energies for ET sites in proteins range from 0.25 to 1 eV (*37*).

The analytical solution of Scheme 2 (eq S3 in the Supporting Information) gives the equation for the catalytic wave in the ideal case where interfacial ET rates are the same for all adsorbed enzyme molecules. This equation involves five parameters: the limiting current, two reduction potentials ($E_{O/I}$, and $E_{I/R}$), and $(k_2/k_0{}^{O/I})^{app}$ and $(k_2/k_0{}^{I/R})^{app}$. The reduction potentials are as defined in Scheme 2, and the $(k_2/k_0)^{app}$ terms are *apparent* parameters derived from k_2 (the first-order, potential-independent rate constant for hydrogen formation and release by the fully reduced and protonated active site) and $k_0{}^{O/I}$ and $k_0{}^{I/R}$ (the interfacial ET rate constants at zero

[4] The oxidation of the active site Ni_a-S to the inactive, ready state Ni_r* occurs at −104 and −157 mV at pH 7, 45 °C, 1 and 0.01 bar of H_2, respectively, for *A. vinosum* [NiFe]-hydrogenase (A. K. Jones, S. E. Lamle, H. Pershad, K. A. Vincent, S. P. J. Albracht, and F. A. Armstrong, manuscript in preparation) and at approximately −110 mV at pH 7, 40 °C, in the absence of hydrogen, for the enzyme from *D. gigas* (*32*).

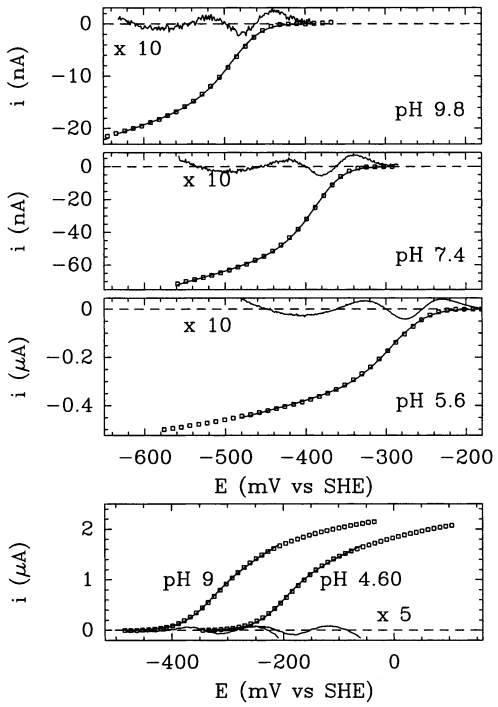

FIGURE 5: Catalytic voltammograms (squares, only one experimental point in every 10 collected has been plotted), best fits to eq S9, and residuals (enlarged) for proton reduction at three different pH values (upper panels) and hydrogen oxidation at two different pH values (bottom panel). Experimental conditions are as described in Figure 2.

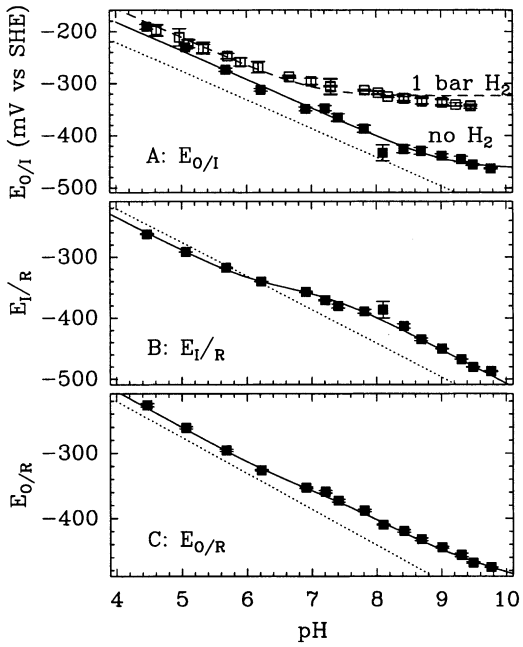

FIGURE 6: Reduction potential of the active site of *A. vinosum* [NiFe]-hydrogenase measured (□) in the presence of H_2 (i.e., obtained from H_2 oxidation waves) or (■) in the absence of H_2 (i.e., obtained from H^+ reduction waves). Filled squares in panels A and B are the two reduction potentials obtained by fitting proton reduction voltammograms such as those shown in Figure 5 to eq S9. Conditions are as described in Figure 2. In panel C, $E_{O/R}$ is the average of $E_{O/I}$ and $E_{I/R}$. Error bars correspond to the difference between the parameters determined for scanning in the oxidative and the reductive directions. The solid lines are fits to eqs S12 (A), S11 (B), and S13 (C). The dashed line in panel A is the best fit to eq S14. The parameters obtained by fitting these pH dependences are reported in Table 1. The dashed line is the potential of the H^+/H_2 couple under 1 bar of H_2 to provide a reference line with a slope of −55 mV/pH (one-proton:one-electron). This potential is not related to the shape or position of the proton reduction wave in the absence of H_2.

overpotential). In the following analysis, we assume that $(k_2/k_0^{O/I})^{app}$ and $(k_2/k_0^{I/R})^{app}$ are equal (this assumption is justified at the end of the Supporting Information).

Since disorder among the adsorbed enzyme molecules introduces a dispersion of interfacial ET rate constants, the last step in the derivation of the current equation is to average this ideal current over a *distribution* of values of k_0, rather than a single value (Supporting Information and ref *33*). The catalytic voltammogram was then fit to eq S9 with four adjustable parameters: two reduction potentials, a parameter describing the competition between interfacial ET and turnover (k_2/k_0^{max}), and $i_{lim}/\beta d_0$, where βd_0 is a geometric parameter linked to the distribution of interfacial ET rates due to distance and electronic coupling.

Equation S9 allowed successful fitting of the catalytic waveshapes for H^+ reduction (upper panels in Figure 5), and the values of the two adjustable reduction potentials over the entire pH range studied are collected together in Figure 6 (■ in panels A and B). Although the Levich plots in Figure 3B show that the current is slightly mass-transport controlled even at the highest rotation rates investigated, the fits of the voltammograms recorded at 4000 and 6000 rpm gave virtually identical parameters (data not shown).

The fits of the pH dependences of the reduction potentials to eqs S11−S13 (Supporting Information) gave the acidity constants that are collated in Table 1. The protonation pattern that successfully accounts for the pH dependence of the two reduction potentials requires the binding of up to *three* protons, as depicted in Scheme 3A.

Similar experiments were conducted at 5, 30, and 45 °C, and no significant differences were noticed for the relative pH dependences of the reduction potentials over this range. At 45 °C, both reduction potentials ($E_{O/I}$ and $E_{I/R}$) were shifted by approximatively −40 mV with respect to the values measured at 5 °C.

Proton Reduction: pH Dependence of the Limiting Current. Since interfacial ET rates increase with overpotential (exponentially at small driving force), they eventually exceed k_2. Under this condition, and provided intramolecular ET through the FeS clusters is fast, as expected (*38*), the active site will tend toward 100% reduction at steady state, and the change in limiting current as a function of pH reveals the protonation equilibria between the different protonation states of the fully reduced active site, along with their relative activities. If the most protonated, fully reduced state ($R:3H^+$ in Scheme 3) were the only species functional in proton reduction (with a rate constant $k_2^{R:3H}$), the limiting current would follow the relationship

$$i_{lim}^{\omega=\infty} \propto \frac{k_2^{R:3H}}{1+\frac{K_{R:2H}}{[H^+]}\left(1+\frac{K_{R:H}}{[H^+]}\right)} \qquad (2)$$

and the activity would drop sharply at pH values above $pK_{R:2H} \approx 6.5$. That this is not the case is clear from Figure 4, in which there is significant residual current at high pH values[5] that is not accounted for by eq 2 (dashed line). In

Table 1: Thermodynamic Properties of the Active Site of *A. vinosum* [NiFe]-Hydrogenase at 5 °C[a]

pK_O	7.4 ± 0.2[b]		
pK_I	9.1 ± 0.1[c]		
$pK_{I:H}$	7.1 ± 0.1[d]		
$pK_{R:H}$	9.0 ± 0.1[b]	9.25 ± 0.3[e]	
$pK_{R:2H}$	6.5 ± 0.2[b]	6.2 ± 0.1[d]	6.25 ± 0.2[e]
$pK_{I:H2}$	7.0 ± 0.1[f]		

[a] The *pK* s are as defined in Scheme 3. [b] From the fit of $E_{O/R}$ to eq S13, Figure 6C. [c] From the fit of $E_{O/I}$ to eq S12, Figure 6A. [d] From the fit of $E_{I/R}$ to eq S11, Figure 6B. [e] From the fit of $i_{-560}{}^{\omega=\infty}$ to eq 3, solid line in Figure 4. [f] From the fit of $E_{O/I}$ to eq S14, dashed line in Figure 6A.

Scheme 3: Protonation Pattern and Turnover Scheme Implied by the Modeling of Data for Proton Reduction (in the Absence of Bulk H_2) (A) or under a Saturating Concentration of H_2 (B)[a]

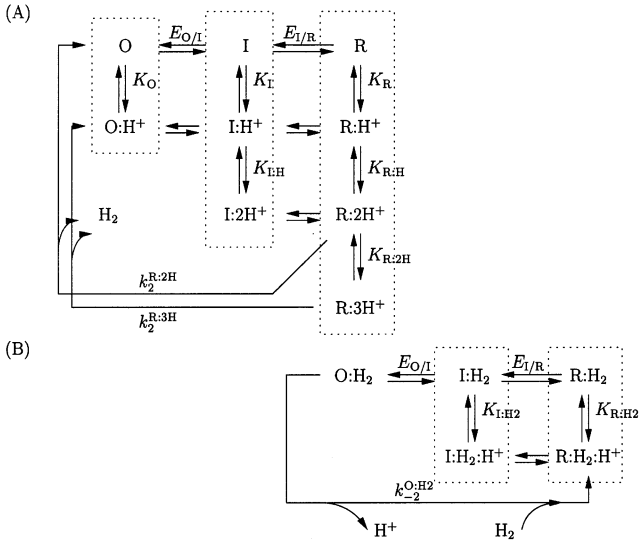

[a] Species within dotted boxes remain at equilibrium.

terms of the protonation patterns discussed above, i.e., that *R* exists in three different protonation states, this suggests that turnover can occur from two different protonation states of the enzyme, as shown in Scheme 3. The limiting current is then given by

$$i_{\lim}{}^{\omega=\infty} \propto \frac{k_2{}^{R:3H} + k_2{}^{R:2H}\left(\frac{K_{R:2H}}{[H^+]}\right)}{1 + \frac{K_{R:2H}}{[H^+]}\left(1 + \frac{K_{R:H}}{[H^+]}\right)} \qquad (3)$$

where $k_2{}^{R:3H}$ and $k_2{}^{R:2H}$ represent the turnover numbers from the two protonation states able to undergo catalysis, and $K_{R:2H}$ and $K_{R:H}$ represent the acidity constants of $R:2H^+$ and $R:H^+$, respectively. The fit of $i_{-560}(pH)/i_{-560}(pH = 6.6)$ is shown in Figure 4; it gives $k_2{}^{R:3H}/k_2{}^{R:2H} = 10 \pm 1$, $pK_{R:2H} = 6.25 \pm 0.2$, and $pK_{R:H} = 9.25 \pm 0.3$. As shown in Table 1, the latter parameters are in excellent agreement with those determined independently by fitting the pH dependences of the reduction potentials (see Supporting Information).

[5] This current is on the order of 0.1−1 μA and is clearly distinguishable from any nonfaradaic charging current, which is at most on the order of 10 nA.

Hydrogen Oxidation: Catalytic Waveshape. The same approach as used for proton reduction allows the catalytic waves for hydrogen oxidation to be interpreted.

When the voltammograms were fit to eqs S9a−S10 (see Supporting Information), the adjusted value of $E_{I/R}$ was systematically found to lie *below* the potential range where a catalytic current is measured. This implies that the value of this reduction potential cannot be determined from the catalytic voltammograms. Therefore, to fit the data, we used a modified version of eq S10, where the terms $\exp[F/RT(E_{I/R} - E)]$ are fixed to zero, leaving three adjustable parameters ($E_{O/I}$, $k_{-2}/k_0{}^{max}$, and $i_{lim}/\beta d_0$). The fits of the catalytic waves for hydrogen oxidation are shown in the lower panel of Figure 5.

The pH dependence of $E_{O/I}$ measured from the fit for catalytic hydrogen oxidation (under 1 atm of H_2) is shown in Figure 6A (□). The dashed line is the best fit to eq S14, which gives the acidity constant of the half-reduced active site bound to hydrogen, $pK_{I:H2} = 7 \pm 0.1$ (Table 1).

DISCUSSION

General Considerations. Whereas solution kinetic studies of [NiFe]-hydrogenases are complicated by the slow interaction with soluble redox dyes, our previous protein film voltammetry study of *A. vinosum* [NiFe]-hydrogenase showed that the PGE electrode serves as a very fast artificial redox partner (*25*). This has opened new and alternative opportunities to study, simultaneously, the energetics and kinetics of the catalytic processes, and in the present work, we have focused on the mechanism of hydrogen evolution and oxidation by the fully active enzyme. The study of the (in)-activation of the enzyme under conditions of strict potential control will be reported elsewhere (A. K. Jones, S. E. Lamle, H. Pershad, K. A. Vincent, S. P. J. Albracht, and F. A. Armstrong, manuscript in preparation). The study of hydrogen oxidation as a function of temperature is reported in ref *33*.

Proton reduction activity is low in the presence of hydrogen, but intense catalytic reductive currents are measured under a N_2 atmosphere, even at a temperature as low as 5 °C (Figure 2). The facts that the slopes of the Koutecky−Levich plots in Figure 3C are pH-independent and that the catalytic current does not depend on buffer concentration together make proton depletion at the electrode surface a very unlikely explanation for why there is an increase in limiting current as the electrode rotation rate (ω) is raised (Figure 3A). This must instead result from dispersal of the product (H_2), and therefore a decrease in product (hydrogen) inhibition. Thus, while rotating the electrode is normally used as a way to increase the supply of diffusing species from the bulk solution to the electrode surface (*25*, *28*−*30*), in the present case, electrode rotation is exploited to observe and to control product inhibition and dispersal.

The inhibition of proton reduction by bulk hydrogen enables oxidative catalysis to be studied without complications due to proton reduction. Therefore, in either direction—i.e., proton reduction (hydrogen absent from the bulk solution and use of a fast electrode rotation rate) and hydrogen oxidation (under H_2-saturating conditions and fast rotation rate)—the catalytic reaction is rendered unidirectional.

The modeling of catalytic voltammograms was based on the steady-state solution of schemes derived from Scheme 2

(Supporting Information), according to which the active site exists in three different redox states [oxidized (O), half-reduced (I, intermediate), and reduced (R)], which can be considered to interconvert as a result of long-range, one-electron transfers with the electrode, coupled proton transfers, and two-electron $2H^+/H_2$ transformations. By fitting the catalytic voltammograms (Figure 5), the reduction potentials of the active site can be measured at room temperature, in the presence of either substrate, while the enzyme is turning over (Figure 6). The variation in high- or low-potential limiting current as a function of pH (Figure 4) represents the activity profile for hydrogen oxidation or evolution, respectively.

Mechanistic Implications: Proton Reduction. Two p*K* values are clearly apparent from the variation with pH of H^+-reduction activity measured at low potential (−560 mV, solid symbols in Figure 4), and this shows that two different protonation states of the most reduced form of the enzyme are able to reduce protons and release H_2. This seems to be common in hydrogenases, as residual activity at high pH appears in earlier reports on the pH dependence of the proton reduction rate (*39*−*41*).

By fitting both the limiting currents and waveshapes as a function of pH, we deduced the proton binding sequence (Scheme 3A) and determined the acidity constants of the different intermediates (Table 1). At all but very alkaline pH values, the reduction and protonation events follow a compulsory sequence of one-electron:one-proton transfers. Indeed, at pH $\lesssim$ 7 where activity is highest, $O:H^+$ is reduced to $I:2H^+$ and then to $R:3H^+$, while at pH values between 7 and 9 (lower activity), O is reduced to $R:2H^+$ via $I:H^+$. (This is probably important for preserving electrical neutrality in the low-dielectric medium surrounding the active site.) These results show that a labile proton in the active site, with acidity constant $pK_a \approx 7$, enhances the activity about 10-fold ($k_2^{R:3H}/k_2^{R:2H} \approx 10$, Figure 4). Whereas the involvement of three protons in the catalytic cycle has already been proposed on the basis of the pH dependence of reduction potentials measured by EPR titrations (*42*, *43*), our proposal is *not* that three protons are coupled to the transfer of two electrons in the proton reduction cycle but that a supernumerary proton is taken up by the active site in *all* its redox states below pH 7.

Mechanistic Implications: Inhibition of Reductive Activity by Hydrogen. Inhibition of H^+ reduction under 1 bar hydrogen is demonstrated by the large, instantaneous attenuation of the proton reduction current when H_2 is introduced into the cell and accounts for the rotation-rate dependence of the catalytic current in the absence of bulk hydrogen.

The following options can be considered to explain the inhibition by H_2. The first is that binding of H_2 occurs to the most reduced state R and prevents release of the product. The second option is that binding of H_2 occurs much more tightly to either of the more oxidized forms (O and I) than to R, the effect of which is to cause a large decrease in the reduction potential of these species, and hence a shift of the reductive wave to lower electrode potential.

We consider first the second option. Under 1 bar of H_2, the value of $E_{O/I}$ actually *increases* slightly (compare solid and open symbols in Figure 6A); consequently, in terms of our above-mentioned assignment, H_2 binds less tightly to O than to I. We need then to distinguish whether binding occurs preferentially to I or R. If the former were true, it would be possible to induce release of H_2 (and thus to overcome H_2 inhibition) by lowering the electrode potential further to a value commensurate with that of the redox couple I/R with H_2 bound. We found that even at −760 mV (at pH 6, 5 °C, 1 bar of H_2), i.e., 400 mV more negative than the position of the wave without H_2, there was no evidence for any recovery of activity. If 1 bar of H_2 caused a shift of at least −400 mV, it follows that 0.1 bar of H_2 would produce a shift of at least −340 mV, and there would be a large separation between the waves for H^+ reduction and H_2 oxidation. This is not the case, since under 0.1 bar of H_2 the reactions in both directions occur at electrode potentials very close to $E^{0\prime}_{H^+/H_2}$ (see Figure 4 in ref 25), so that the second option can be excluded. Therefore, the reason for the loss of reductive activity under 1 bar of H_2 is that the product of the reaction binds strongly to R and prevents product release. According to the first option above, the main effect of H_2 is to attenuate the current rather than shift the potential required to elicit H+ reduction catalysis.

Mechanistic Implications: Hydrogen Oxidation. The analysis of the catalytic waveshapes allows both one-electron reduction potentials of the active site to be measured from turnover experiments only if they are close to each other (see Supporting Information). Therefore, the "one-electron shape" of the catalytic waves for hydrogen oxidation (only $E_{O/I}$ could be measured) suggests that I is (at least slightly) stabilized upon hydrogen binding. At low pH, in the *absence* of bulk hydrogen, the difference between the reduction potentials of the O/I and I/R transitions is about 65 mV (Figure 6). A 10-fold preferential binding of H_2 to I compared to R would be enough to increase this difference to 120 mV under 1 bar of hydrogen (thus making the catalytic waveshape for hydrogen oxidation insensitive to the value of $E_{I/R}$).

Two observations are particularly important. First, 1 bar of hydrogen is sufficient to saturate both the reduced (R) and oxidized (O) catalytic states of the enzyme [see above and note that K_m for hydrogen oxidation is estimated at approximatively 1% H_2], and second, H_2 has only a small influence on the reduction potential of the O/I transition (Figure 6A), showing that the affinity of the active site for hydrogen is hardly changed upon oxidation of I. Together these suggest that under 1 bar of H_2, the substrate (a dihydrogen molecule, or equivalently a proton:hydride pair) is bound to the active site in *all* its redox states. Scheme 3B depicts the catalytic sequence of events deduced from the pH dependence of the waveshape for hydrogen oxidation.

In Scheme 3, the upper catalytic cycle, which accounts for H^+ reduction, is therefore distinct from that deduced from H_2 oxidation experiments carried out under H_2-saturating conditions. This simply means that the states of the active site involved in either catalytic process can be considered as different species depending on whether H_2 is bound. It is therefore natural that two cycles can emerge, one accounting for each catalytic direction (Scheme 3). Note that these two cycles should be linked by binding of a H_2 molecule and possibly the release of protons; but the exact connection is not established, as the protonation pattern during oxidative

Table 2: Literature Values for the Reduction Potentials of the Ni_a-S/Ni_a-C* and Ni_a-C*/Ni_a-SR Transitions[a]

	Ni_a-S/Ni_a-C*	Ni_a-C*/Ni_a-SR	pH	ref
D. gigas[b]	−330 (−47)	−400 (−43)	7	32
D. gigas[c]	−270 (−120)	−390 (−60)	7	42
D. gigas	−330	−405	8	46
D. gigas	−330	−370	8	43
A. vinosum		−458	8	27
A. vinosum[d]	−345	−360	7	*e*

[a] All potentials are given in millivolts versus SHE; pH dependence is indicated in parentheses. [b] Measured at 40 °C over the pH range 5.5−8. (at 40 °C, a one-electron:one-proton reduction potential should decrease by −62 mV/pH). [c] In the pH range ≈5.8−8.2. [d] From the analysis of catalytic waveshapes obtained at 5 °C in the absence of bulk hydrogen. [e] This work.

turnover cannot be entirely determined from the experiments presented in this paper.[6]

The pH dependence of $E_{O/I}$ under 1 bar of H_2 is shown (□) in Figure 6A; proton release from the active site upon oxidation of I occurs only at pH < 7. Indeed, the $pK_a \approx 7$ detected in the pH dependence of $E_{O/I}$ must correspond to a proton in the half-reduced active site bound to hydrogen (I). Since the shapes of the catalytic waves under 1 bar of H_2 reveal only the I to O oxidation ($E_{I/R}$ could not be measured under 1 bar of H_2), it was unfortunately not possible to detect the deprotonation event(s) following the first one-electron oxidation of R bound to hydrogen.

No protonation equilibria were detected for the oxidized active site bound to hydrogen ($O:H_2$ in Scheme 3B). This is fully consistent with the fact that the rate of hydrogen oxidation at high driving force is pH-independent (□ in Figure 4; lower panel in Figure 5). This observation is unambiguous and contrasts with earlier reports on the pH dependence of hydrogen oxidation rates by hydrogenases (*39*, *44*, *45*), and suggests that these assays were complicated by the rate-limiting and pH-dependent active-site oxidation by the redox mediators. With PFV, the enzyme activity is controlled directly by the electrode potential, and by increasing the driving force, it is easy to ensure that the true limiting rate is measured.

Proposal for the Mechanisms. Since the most common proposal for the mechanism involves the participation of Ni_a-S, Ni_a-C*, and Ni_a-SR in the catalytic cycle (Scheme 1), the most obvious assignments of the species detected in the voltammetry are that O is Ni_a-S, I is Ni_a-C*, and R is Ni_a-SR, each subject to different affinities for H^+ and H_2. At pH 7, we measured $E_{O/I} = -345$ mV and $E_{I/R} = -360$ mV vs SHE (Figure 6), and we note that these values are in the range reported for the reduction potentials of the different active states of the [NiFe]-hydrogenase active site (Table 2). In the following discussion, we will follow this line of correspondence while remaining critical as to exact interpretations. To simplify our analysis, we have not considered the possibilities that the Fe-S clusters may play roles additional to relaying electrons.

[6] For example it is not clear whether the state $O:H_2$ is equivalent in composition to $R:2H^+$ or $R:3H^+$. This connection between the cycles for oxidative and reductive catalysis should not be confused with that proposed by Roberts and Lindahl (*43*). These authors consider the redox states of the FeS clusters and draw distinct cycles depending on the total "electron loading" of the enzyme, whereas the model presented in our work takes into account only the chemistry occurring at the [NiFe] active site.

The use of PFV, together with the general methods for interpreting quasi-sigmoidal catalytic waves developed in the Supporting Information, provides a unique opportunity to study the energetics of the catalytic cycle. The reduction potentials of the active site in the presence of either of its substrates could be measured at ambient temperatures and during turnover (Figure 6), and their pH dependences allow measurement of the affinities of the different forms of the active site for protons and determination of the sequence of coupled protonation steps. The pH dependences reported here contrast with those measured from titrations either with dyes (*32*) or dyes and H_2 (*42*) or under He/H_2 mixed atmospheres (*27*, *47*); these apparent discrepancies are likely to reflect equilibrium versus dynamic behaviors of the system. The sequence of proton and electron transfers during the catalytic cycle is dependent both on pH (Scheme 3 and Table 1) and on the catalytic directions.

Under a N_2 atmosphere, O is reduced to $R:2H^+$ at $7 < pH < 9$ or $O:H^+$ is reduced to $R:3H^+$ at pH < 7. This is consistent with the observation that the isolated and spectroscopically characterized states of the active site generally exist in two forms depending on pH, with an extra proton being added to the active site at low pH, withdrawing some electron density and thereby shifting the CO band to higher frequencies.[7] (*32*, *48*). The reduction involves two one-electron, one-proton uptakes at all pH values, but the rate of H^+ reduction under a N_2 atmosphere is pH-dependent and enhanced about 10-fold by this labile active-site proton (the pK_a of which is ≈7; Figure 4 and Table 1). This exchangeable proton is unlikely to be the hydrogen species that dissociates from the Ni_a-C* state upon illumination (*12*, *49*), since (i) the EPR signal of Ni_a-C* (*g*-values and line widths) shows little pH dependence (*27*, *47*) and (ii) illumination results in a *large* increase of the electron density on the metal atoms (*8*, *50*). The light-sensitive species might instead be a spectator (nonreacting) dihydrogen molecule bound to the active site.

The low-pH, H_2-free, oxidized form of the active site ($O:H^+$ in Scheme 3A) most likely corresponds to Ni_a-S, i.e., $Fe^{II}Ni^{II}$, with a proton bound to a base (Ba) in the active site. $O:H^+$ ($Fe^{II}Ni^{II}BaH$) and the high-pH form O ($Fe^{II}Ni^{II}Ba^-$) might correspond respectively to the SI_{1934} and SI_{1914} forms of the enzyme from *D. gigas* (*32*). The first one-electron: one-proton reduction of $O:H^+$ produces an $Fe^{II}Ni^{I}H^+BaH$ state that converts immediately to Ni_a-C* containing a bound hydride ($I:2H^+$), i.e., $Fe^{II}Ni^{III}H^-BaH$ (note that, alternatively, the first electron uptake could lead to unstable Fe^{I}). Subsequent one-electron:one-proton reduction leads to $R:3H^+$ ($Fe^{II}Ni^{II}H^+H^-BaH$), in equilibrium with the 10-fold less active, deprotonated form $R:2H^+$ ($Fe^{II}Ni^{II}H^+H^-Ba^-$) and the alkaline, inactive form $R:H^+$ ($Fe^{II}Ni^{II}H^-Ba^-$) that may

[7] In the absence of H_2, this has been reported for the Ni_a-S and (H_2-free) Ni_a-SR states of *D. gigas* (*32*) and *D. desulfuricans* (*48*) [NiFe]-hydrogenases. The CO stretching bands of the enzyme from *A. vinosum* under H_2 also show an apparent pH dependence: the band at 1937 cm^{-1} from the Ni_a-SR state and that at 1951 cm^{-1} from the Ni_a-C* state are stronger at pH 6 than at pH 9, whereas the 1921 cm^{-1} band of the Ni_a-SR state is weaker. In addition, a small band at 1913 cm^{-1} was observed at pH 9 but not at pH 6 (B. Bleijlevens and S. P. J. Albracht, unpublished results). However, no pH dependence was observed for the IR or EPR signals of the Ni_a-S and Ni_a-C* states of *A. vinosum* [NiFe]-hydrogenase (B. Bleijlevens and S. P. J. Albracht, unpublished results).

correspond to the state of the enzyme having a small IR band at 1913 cm^{-1}.[7] The formation (from H^+ and H^-) and release of H_2 by the reduced, active forms regenerates O:H^+ or O.

Our state R:3H^+ ($Fe^{II}Ni^{II}H^+H^-$BaH) could apply to two different species depending on whether the H−H bond is already formed. Under one bar hydrogen, inhibition of proton reduction proceeds by preventing the release of H_2 from the reduced, active forms, $Fe^{II}Ni^{II}H_2$Ba(H).

For hydrogen oxidation, our results show that, under 1 bar of H_2, the active site is saturated in all its redox states, i.e., throughout the catalytic cycle. (In the future, a complete study as a function of the hydrogen pressure could be undertaken to determine, precisely, the affinity of each redox state for H_2.) The one-electron oxidations of the reduced form lead first to Ni_a-C* (i.e., I:H_2 with or without H^+ p$K \approx 7$, in Scheme 3), $Fe^{II}Ni^{III}H_2$ or $Fe^{II}Ni^{III}H^+H^-$, and then to the fully oxidized form O:H_2 ($Fe^{II}Ni^{II}2H^+$) via an unstable intermediate, possibly $Fe^{III}Ni^{II}H^+H^-$.

Importantly, by use of whatever driving force is required to push the reaction in either direction, it is possible to access different unstable intermediates in the catalytic cycles for H^+ reduction or H_2 oxidation (e.g., $Fe^{II}Ni^{I}$ and $Fe^{III}Ni^{II}$, respectively). Microscopic reversibility is not a requirement since energy input is necessarily provided to drive catalysis: rates are measured over a potential range of nearly 1 V (−760 to +350 mV vs SHE).

Final Remarks. Importantly, the present study reveals the energetics of the entire catalytic cycles for proton reduction and hydrogen oxidation and provides a perspective that is complementary to that obtained from solution titrations with redox dyes as the sole reductant (i.e., without a defined H_2 pressure): these titrations can be difficult to interpret, because one of the substrates, the proton, is inevitably present in the titration medium. Whereas this does not impede the titration of oxidized, inactive forms of the enzyme, protons compete with dyes for the redox transformation of active states that are sufficiently reduced to produce and release hydrogen (*51*). Under these conditions of *assay*—as opposed to equilibrium titration—rapid turnover of protons can lead to a significant concentration of the oxidized form of the active site, even if a platinum electrode interacting with the mediators indicates a very low potential. In these "out of equilibrium titrations," it is difficult to ascertain whether a steady state is achieved (the rate is not measured), and were this to be the case, it would be difficult also to ensure that the measured quantities correspond to equilibrium properties (*51*).

Furthermore, kinetic properties of the activities of hydrogenases can be complicated by the slow exchange of electrons between the enzyme and the soluble redox partner. Provided intramolecular ET is fast, these problems are not encountered with PFV. The electrode provides the important ability to increase the rate of delivery of electrons to or from the active site (by lowering or raising the electrode potential, respectively) to whatever value is required to compete successfully with turnover of substrate. Importantly, also, the overpotential for direct (nonenzymatic) reduction of protons on graphite is large enough that this process does not interfere with the catalytic current. It is therefore possible to achieve a true titration of the active site in the presence of substrate (see Supporting Information and ref *22*) and to measure activities, in either direction, that are not limited by the thermodynamic driving force of a soluble redox agent.

ACKNOWLEDGMENT

We thank B. Audit, P. L. Dutton, B. Guigliarelli, V. Guirardel, L. J. C. Jeuken, H. R. Pershad, A. W. Rutherford, and C. A. Salgueiro for fruitful discussions.

SUPPORTING INFORMATION AVAILABLE

General method to interpret catalytic voltammograms, together with the detailed analysis of the pH dependences presented in Figure 6. This material is available free of charge via the Internet at http://pubs.acs.org.

REFERENCES

1. Albracht, S. P. J. (1994) *Biochim. Biophys. Acta 1188*, 167−204.
2. Adams, M. W. W. (1990) *Biochim. Biophys. Acta 1020*, 115−145.
3. Cammack, R., Frey, M., and Robson, R., Eds. (2001) *Hydrogen as a Fuel, Learning from Nature*, Taylor and Francis, London and New York.
4. Volbeda, A., Charon, M. H., Piras, C., Hatchikian, E. C., Frey, M., and Fontecilla-Camps, J. C. (1995) *Nature 373*, 580−587.
5. Volbeda, A., Garcia, E., Piras, C., De Lacey, A. L., Fernandez, V. M., Hatchikian, E. C., Frey, M., and Fontecilla-Camps, J. C. (1996) *J. Am. Chem. Soc. 118*, 12989−12996.
6. Happe, R. P., Roseboom, W., Pierik, A. J., Albracht, S. P. J., and Bagley, K. A. (1997) *Nature 385*, 126−126.
7. Surerus, K. K., Chen, M., van der Zwaan, J. W., Rusnak, F. M., Kolk, M., Duin, E. C., Albracht, S. P. J., and Münck, E. (1994) *Biochemistry 33*, 4980−4993.
8. Happe, R. P., Roseboom, W., and Albracht, S. P. J. (1999) *Eur. J. Biochem. 259*, 602−608.
9. Davidson, G., Choudhury, S. B., Gu, Z., Bose, K., Roseboom, W., Albracht, S. P. J., and Maroney, M. J. (2000) *Biochemistry 39*, 7468−7479.
10. Dole, F., Fournel, A., Magro, V., Hatchikian, E. C., Bertrand, P., and Guigliarelli, B. (1997) *Biochemistry 36*, 7847−7854.
11. Huyett, J. E., Carepo, M., Pamplona, A., Franco, R., Moura, I., Moura, J. J. G., and Hoffman, B. M. (1997) *J. Am. Chem. Soc. 119*, 9291−9292.
12. Maroney, M. J., and Bryngelson, P. A. (2001) *J. Biol. Inorg. Chem. 6*, 453−459.
13. Siegbahn, P. E. M., Blomberg, M. R. A., Wirstam, M., and Crabtree, R. H. (2001) *J. Biol. Inorg. Chem. 6*, 460−466.
14. Fan, H.-J., and Hall, M. B. (2001) *J. Biol. Inorg. Chem. 6*, 467−473.
15. Frey, M. (2002) *ChemBioChem 3*, 153−160.
16. Armstrong, F. A., Heering, H. A., and Hirst, J. (1997) *Chem. Soc. Rev. 26*, 169−179.
17. Armstrong, F. A., and Wilson, G. S. (2000) *Electrochim. Acta 45*, 2623−2645.
18. Heering, H. A., Weiner, J. H., and Armstrong, F. A. (1997) *J. Am. Chem. Soc. 119*, 11628−11638.
19. Pershad, H. R., Hirst, J., Cochran, B., Ackrell, B. A. C., and Armstrong, F. A. (1999) *Biochim. Biophys. Acta 1412*, 262−272.
20. Butt, J. N., Thornton, J., Richardson, D. J., and Dobbin, P. S. (2000) *Biophys. J. 78*, 1001−1009.
21. Heffron, K., Léger, C., Rothery, R. A., Weiner, J. H., and Armstrong, F. A. (2001) *Biochemistry 40*, 3117−3126.
22. Léger, C., Heffron, K., Pershad, H. R., Maklashina, E., Luna-Chavez, C., Cecchini, G., Ackrell, B. A. C., and Armstrong, F. A. (2001) *Biochemistry 40*, 11234−11245.
23. Bateman, L., Léger, C., Goodin, D. B., and Armstrong, F. A. (2001) *J. Am. Chem. Soc. 123*, 9260−9263.
24. Anderson, L. J., Richardson, D. J., and Butt, J. N. (2001) *Biochemistry 40*, 11294−11307.
25. Pershad, H. R., Duff, J. L. C., Heering, H. A., Duin, E. C., Albracht, S. P. J., and Armstrong, F. A. (1999) *Biochemistry 38*, 8992−8999.
26. Jones, A. K., Sillery, E., Albracht, S. P. J., and Armstrong, F. A. (2002) *Chem. Commun.*, 866−867.
27. Coremans, J., van Garderen, C. J., and Albracht, S. P. J. (1992) *Biochim. Biophys. Acta 1119*, 148−156.
28. Sucheta, A., Cammack, R., Weiner, J., and Armstrong, F. A. (1993) *Biochemistry 32*, 5455−5465.

29. Bard, A. J., and Faulkner, L. R. (2001) *Electrochemical methods. Fundamentals and applications*, 2nd ed., John Wiley & Sons, Inc.
30. Heering, H. A., Hirst, J., and Armstrong, F. A. (1998) *J. Phys. Chem. B 102*, 6889−6902.
31. De Lacey, A., Moiroux, J., and Bourdillon, C. (2000) *Eur. J. Biochem. 267*, 6560−6570.
32. De Lacey, A. L., Hatchikian, E. C., Volbeda, A., Frey, M., Fontecilla-Camps, J. C., and Fernandez, V. M. (1997) *J. Am. Chem. Soc. 119*, 7181−7189.
33. Léger, C., Jones, A. K., Albracht, S. P. J., and Armstrong, F. A. (2002) *J. Phys. Chem. B* (in press).
34. Chidsey, C. E. D. (1991) *Science 251*, 919−922.
35. Weber, K., and Creager, S. E. (1994) *Anal. Chem. 66*, 3164−3172.
36. Tender, L., Carter, M. T., and Murray, R. W. (1994) *Anal. Chem. 66*, 3173−3181.
37. Sigfridsson, E., Olsson, M. H. M., and Ryde, U. (2001) *J. Phys. Chem. B 105*, 5546−5552.
38. Page, C. C., Moser, C. C., Chen, X., and Dutton, P. L. (1999) *Nature 402*, 47−52.
39. Zorin, N. A., Dimon, B., Gagnon, J., Gaillard, J., Carrier, P., and Vignais, P. M. (1996) *Eur. J. Biochem. 241*, 675−681.
40. Fernandez, V. M., Aguirre, R., and Hatchikian, E. C. (1984) *Biochim. Biophys. Acta 790*, 1−7.
41. van Dijk, C., and Veeger, C. (1981) *Eur. J. Biochem. 114*, 209−219.
42. Cammack, R., Patil, D. S., Hatchikian, E. C., and Fernandez, V. M. (1987) *Biochim. Biophys. Acta 912*, 98−109.
43. Roberts, L. M., and Lindahl, P. A. (1994) *Biochemistry 33*, 14339−14350.
44. Vignais, P. M., Henry, M. F., Berlier, Y., and Lespinat, P. A. (1982) *Biochim. Biophys. Acta 681*, 519−529.
45. Lespinat, P., Berlier, Y., Fauque, G., Czechowski, M., and LeGall, J. (1986) *Biochimie 68*, 55−61.
46. Roberts, L. M., and Lindahl, P. A. (1995) *J. Am. Chem. Soc. 117*, 2565−2572.
47. Coremans, J., van der Zwaan, J. W., and Albracht, S. P. J. (1992) *Biochim. Biophys. Acta 1119*, 157−168.
48. DeLacey, A. L., Stadler, C., Fernandez, V. M., Hatchikian, E. C., Fan, H.-J., Li, S., and Hall, M. B. (2002) *J. Biol. Inorg. Chem. 7*, 318−326.
49. Bleijlevens, B., Faber, B. W., and Albracht, S. P. J. (2001) *J. Biol. Inorg. Chem. 6*, 763−769.
50. Bagley, K. A., van Garderen, C. J., Chen, M., Duin, E. C., Albracht, S. P. J., and Woodruff, W. H. (1994) *Biochemistry 33*, 9229−9236.
51. Pierik, A. J., Hagen, W. R., Redeker, J. S., Wolbert, R. B. G., Boersma, M., Verhagen, M., Grande, H. J., Veeger, C., Mutsaers, P. H. A., Sands, R. H., and Dunham, W. R. (1992) *Eur. J. Biochem. 209*, 63−72.

BI026586E